

1 **Charge separation in collisions between ice crystals and a spherical**  
2 **simulated graupel of cm-size**

3  
4 Melina Y. Luque, Fernando Nollas, Rodolfo G. Pereyra, Rodrigo E. Bürgesser, Eldo E. Ávila

5 FaMAF, Universidad Nacional de Córdoba, IFEG-CONICET, Córdoba, Argentina

6  
7 **Abstract**

8 This work reports a new laboratory study of the electric charge separated in collisions  
9 between a spherical target of 1 cm in diameter growing by riming and vapor-grown ice crystals,  
10 with the objective of studying the charging behavior of the larger ice precipitation particles in  
11 thunderstorms in terms of the non-inductive mechanism. A series of experiments was conducted  
12 for a wide range of environmental conditions; the measurements were performed for effective  
13 liquid water content between 0.5 and 5 g m<sup>-3</sup>, for ambient temperatures between -5 °C and -30  
14 °C and at air speed of 11 m s<sup>-1</sup>. The magnitude and sign of the electric charge transfer on the ice  
15 sphere as a function of the ambient temperature and the effective liquid water content is  
16 presented. The results show a charge reversal temperature for the riming target which is roughly  
17 independent of liquid water concentration in the measured range. The simulated graupel charges  
18 negatively for temperatures below -15 °C, and positively at temperatures above -15 °C.

19

20

## 21 **1. Introduction**

22 Laboratory studies with all kinds of variations of the environmental parameters have been carried  
23 out to study the non-inductive electrification mechanism. The results of these studies reveal that  
24 parameters such as ambient temperature ( $T_a$ ), liquid water content (LWC) or effective liquid  
25 water content (EW), impact velocity ( $V$ ), droplet and ice crystal size distributions and the  
26 difference in saturation vapor pressures over ice and liquid water may affect sign and magnitude  
27 of the charge acquired by an ice precipitation particle when colliding with ice-crystals  
28 [Takahashi, 1978; Jayaratne et al., 1983; Saunders et al., 1991, 1999, 2001, 2004, 2006; Ávila et  
29 al., 1996; Saunders and Peck, 1998; Ávila and Pereyra, 2000; Pereyra et al., 2000; Ávila et al.,  
30 2013; Luque et al., 2016, 2018].

31 The charging current (CC) that a simulated graupel acquires under collisions with ice  
32 crystals, has been quantified in the laboratory. Typically, the simulated graupel consists of  
33 metallic collectors over which supercooled water droplets hit and freeze, forming an ice cover  
34 that represents the surface characteristic of natural graupels (rime). Dimensions of the simulated  
35 graupel vary from study to study but they usually are around the millimeter-size.

36 Takahashi [1978] rotated a rimed rod of 3 mm in diameter at  $9 \text{ m s}^{-1}$  through a cloud of  
37 ice crystals and supercooled water droplets and measured the CC of the simulated graupel. He  
38 observed that the target may charge negatively or positively depending on the LWC and the  
39 ambient temperature. He found that for temperatures above  $-10 \text{ }^\circ\text{C}$ , the CC was positive for all  
40 LWC values. For temperatures below  $-10 \text{ }^\circ\text{C}$ , the sign of CC showed a dependence with the  
41 value of LWC, being negative for  $0.1 \text{ g m}^{-3} < \text{LWC} < 4 \text{ g m}^{-3}$ , and positive for lower ( $< 0.1 \text{ g m}^{-3}$ )  
42  $)$  and higher LWC values ( $> 4 \text{ g m}^{-3}$ ) regardless of the ambient temperature.

43           Jayaratne et al. [1983] rotated a rimed rod of 5 mm in diameter at  $3 \text{ m s}^{-1}$  and found  
44 significant dependencies of the CC magnitude with the simulated graupel temperature, ice crystal  
45 sizes and the impact velocity. Unlike Takahashi's results, they found a single charge reversal  
46 temperature ( $T_R$ ) as a function of LWC. The rime became positively charged at temperatures  
47 above  $T_R$  and high LWC, and negatively charged at lower LWC or at lower temperatures. The  $T_R$   
48 value was around  $-20 \text{ }^\circ\text{C}$  at  $\text{LWC} = 1 \text{ g m}^{-3}$ .

49           Saunders et al. [1991] measured the CC of a fixed rod of 5 mm in diameter growing by  
50 accretion while it was subjected to collisions with ice crystals in a series of experiments under  
51 controlled conditions at an impact velocity of  $3 \text{ m s}^{-1}$ . They introduced the variable effective  
52 liquid water content (EW) in the place of LWC, EW is the product of LWC and collision  
53 efficiency, therefore, is made up only of those droplets that can be captured by the rod. Thus, this  
54 parameter takes into account the part of the water droplets involved in the riming process. The  
55 EW was varied while the size of the crystals and the impact velocity were kept constant. This  
56 work extended previous measurements by Jayaratne et al. [1983] and modified the charging  
57 diagram (LWC-T) with more than one charge reversal temperature for each LWC.

58           Saunders et al. [1991], Takahashi [1978] and Jayaratne et al. [1983] observed that the  
59 sign of the charge acquired by the simulated graupel mainly depends on the liquid water content  
60 and T. However, their results were different. There were attempts to explain their discrepancies  
61 by recalling that the impact velocities and simulated graupel sizes used were different, but it is  
62 apparent that they could not be the only cause. The differences between the results are still under  
63 debate [Takahashi et al. 2017].

64           Pereyra et al. [2000] carried out measurements of the charge transfer when vapor grown  
65 ice crystals rebound from a riming target representing a graupel pellet falling in a thunderstorm.  
66 Measurements were made at temperatures between  $-5^{\circ}\text{C}$  and  $-30^{\circ}\text{C}$ , at EW values between 0 and  
67  $4 \text{ g m}^{-3}$  and for an impact velocity of  $8.5 \text{ m s}^{-1}$ . Basically, they found positive CC at  $T > -17^{\circ}\text{C}$   
68 and negative CC at  $T < -17^{\circ}\text{C}$ .

69           Ávila and Pereyra [2000] reported measurements using a rod of 4 mm in diameter and  
70 found that the cloud droplet spectrum can affect the EW-T charge diagram of the simulated  
71 graupel. They found that small droplets promote a predominance of positive CC on the simulated  
72 graupel. Bürgesser et al. [2006] used the same experimental device and studied the influence of  
73 the impact velocity on the reversal temperature. They found a shift of the reversal temperature  $T_R$   
74 to warmer temperatures when the impact velocity was increased.

75           Ávila et al. [2013] modified the previous target geometry and carried out their  
76 measurements using as simulated graupel a network constituted by brass wires of 2 mm in  
77 diameter. They measured the CC for lower values of EW representing the microphysical  
78 conditions typically found in the stratiform regions of mesoscale convective systems (MCS). The  
79 results found on this study showed a dependence of the sign of the charge acquired by the  
80 simulated graupel with the impact velocity. Luque et al. [2016] also used the network but in that  
81 case, they measured CC in absence of supercooled water droplets and found a prevalence of  
82 negative charge transfer.

83           Recently, Jayaratne and Saunders [2016] found substantial positive CC when ice crystals  
84 impacted with a rod of 4 mm in diameter under wet growth conditions. Luque et al. [2018]

85 corroborated the results from Jayaratne and Saunders [2016] by working with a spherical  
86 simulated graupel of 1 cm in diameter.

87 Baker et al. [1987] suggested that the sign of the CC acquired by the simulated graupel,  
88 when ice crystals collide with it, is related to the diffusional growth rates of the ice particles  
89 involved in the collision. They proposed that the ice particle growing faster by vapor diffusion  
90 will acquire positive charge while the other particle acquires negative charge. This empirical  
91 observation was supported for many subsequent experimental results [Emersic and Saunders,  
92 2010]. On the other hand, Williams et al. [1991] proposed that simulated graupel being warmed  
93 by riming will charge negatively while a simulated graupel that is not sufficiently warmed by  
94 riming will grow by diffusion and charge positively. Both hypotheses stressed the importance of  
95 the microphysics of the mixed phase clouds to influence the surface state of the interacting  
96 particles. Small changes in the atmospheric conditions or in the microphysical parameters may  
97 affect the surface states of the ice particles and consequently modify the CC sign and magnitude  
98 during the interactions among them.

99 As previously described, in most of the former experimental studies, mm-size graupels of  
100 cylindrical geometry were used. These sizes are surely representative of most of the ice  
101 precipitation particles found in thunderstorms. However, it is well documented that graupel  
102 pellets and hailstones of cm-size can also be present in significant concentrations within  
103 convective regions of mesoscale convective systems and within severe and ordinary  
104 thunderstorms as well; these large ice particles could play a key role in the cloud electrification  
105 processes [Williams, 2001]. There is certainly a need for more laboratory studies of the charge  
106 separation during collisions between ice precipitation particles and ice crystals. Such studies are

107 needed, for example, to determine the charging behavior of larger ice precipitation particles in  
108 thunderstorms in terms of the non-inductive mechanism. Thus, in the present study, the sign and  
109 magnitude of the average charge separated during ice crystal-graupel collisions have been  
110 measured for a simulated graupel of 1 cm in diameter, ambient temperatures between  $-5\text{ }^{\circ}\text{C}$  and  
111  $-30\text{ }^{\circ}\text{C}$ , effective liquid water content between  $0.5$  and  $5\text{ g m}^{-3}$  and impact velocities of  $11\text{ m s}^{-1}$ .

112

## 113 **2. Experimental Setup**

114 The measurements of the charging current were carried out inside a cold chamber using the  
115 experimental setup displayed in Figure 1. The arrangement and the experimental procedure are  
116 the same as those used by Luque et al. [2018].

117 Airflow velocity inside the wind tunnel was controlled with an air pump. Measurements  
118 were performed at an impact velocity  $V = (11 \pm 1)\text{ m s}^{-1}$ , which is representative of the fall speed  
119 of cm-size graupel pellets inside thunderstorms [Heymsfield and Kajikawa, 1987].

120 Three temperatures were recorded during the experiment: the ICC temperature ( $T_{\text{ICC}}$ ), the  
121 wind tunnel temperature ( $T_{\text{WT}}$ ) and the target temperature ( $T_{\text{T}}$ ). These values were sensed using  
122 three previously calibrated thermistors. The location of the thermistors can be seen in Figure 1.  
123 The ICC and target temperatures were recorded only for control and were not used in the data  
124 analysis. The wind tunnel temperature was considered as the ambient temperature for each  
125 experiment, and its variation during the runs was typically less than  $1^{\circ}\text{C}$ .

126

127 A brass sphere target was connected to a current amplifier capable of detecting currents  
128 above 1 pA. The current amplifier output was recorded using an A/D converter.

129 Plastic replicas of ice particles generated in the ICC and cloud particles generated in the  
130 cloud chamber were taken. Clouds were swept with glass slides previously covered with a 3%  
131 Formvar solution following the sampling procedure based on Schaefer [1956]. After analyzing  
132 the samples, size distributions for ice crystals and supercooled droplets were determined.

133 The size distributions of the ice crystals used in the experiments at different temperatures  
134 are displayed in Figure 2. The average size of the crystals varied with T; in fact, at  $-10\text{ }^{\circ}\text{C}$  the  
135 average size is  $15\text{ }\mu\text{m}$ , at  $-13\text{ }^{\circ}\text{C}$  the average size is  $26\text{ }\mu\text{m}$ , at  $-17\text{ }^{\circ}\text{C}$  the average size is  $32\text{ }\mu\text{m}$ ,  
136 at  $-21\text{ }^{\circ}\text{C}$  the average size is  $26\text{ }\mu\text{m}$ , at  $-26\text{ }^{\circ}\text{C}$  the average size is  $19\text{ }\mu\text{m}$  and at  $-30\text{ }^{\circ}\text{C}$  the  
137 average size is  $14\text{ }\mu\text{m}$ . Most of the sampled ice crystals were hexagonal plates with sizes up to  $60$   
138  $\mu\text{m}$ , broad branches ice crystals were observed at  $-13\text{ }^{\circ}\text{C}$  and  $-17\text{ }^{\circ}\text{C}$  with sizes up to  $80\text{ }\mu\text{m}$ .

139 The diameter distributions of the cloud droplets used in the experiments for temperatures  
140 between  $-8\text{ }^{\circ}\text{C}$  and  $-26\text{ }^{\circ}\text{C}$  are displayed in Figure 3. Unlike the ice crystal sizes, droplet sizes do  
141 not show significant variations with temperature. The median diameters of the droplets ranges  
142 between  $14\text{ }\mu\text{m}$  and  $17\text{ }\mu\text{m}$ . Ávila and Pereyra [2000] showed that the size distribution of the  
143 droplets used for riming could affect the sign of the charge transfer to the target. They used two  
144 size distributions A (larger droplets) and B (smaller droplets) to make their point; and found that  
145 larger droplets promote a predominance of negative CC on the target. In the current work, the  
146 laboratory setup used to generate the cloud droplets was the same as those used by Ávila and  
147 Pereyra [2000] to generate the larger size distribution (spectrum A), as well as the droplet size

148 distribution subsequently used by Pereyra et al. [2000], Bürgerser et al. [2006], Ávila et al.  
149 [2013], Luque et al. [2016] and Luque et al. [2018].

150

151 The measurements were performed following the next steps:

- 152 1. Cold chamber temperature was fixed.
- 153 2. Reservoir water temperature was heated up to the desired temperature.
- 154 3. Distilled water droplets were introduced in the ICC for 3 minutes.
- 155 4. Ice crystals were nucleated and they grew by vapor deposition for 60s.
- 156 5. Water reservoir tap was opened to initiate supercooled droplets cloud formation. After 10  
157 seconds, the pump was turned on initiating the airflow inside the wind tunnel. This  
158 airflow drags both clouds from their respective chambers and while the target is growing  
159 by riming, it also collides with the ice crystals.

160 Measurements lasted between 50 and 200 seconds. Complementary experiments were performed  
161 to corroborate that ice crystal concentration remained constant during measurement time.

162

### 163 **3. Results and Discussions**

164 The measurements were performed for ambient temperatures (T) between  $-5\text{ }^{\circ}\text{C}$  and  $-30$   
165  $^{\circ}\text{C}$  and for an impact velocity (V) of  $11\text{ m s}^{-1}$ . The effective liquid water content value (EW) was  
166 determined weighing the accreted mass ( $\Delta M$ ) on the target after each experiment. The accreted  
167 mass relates to the effective liquid water content through the equation:

168 
$$\Delta M = EW V A \Delta t \quad (1)$$

169 where A is cross sectional area of a sphere and  $\Delta t$  is experiment time. The values of EW in this  
170 study ranged between 0.5 and 5 g m<sup>-3</sup> and the uncertainty in the measured EW was typically  
171 about 30%.

172 Figure 4 displays the sign of the charging current (CC) of the target as a function of the  
173 effective liquid water content and the ambient temperature. Open circles indicate T-EW  
174 combinations for which the simulated graupel is charged positively, and filled circles indicate  
175 negative charging of the simulated graupel. The solid line in the lower region of the figure  
176 represents the transition between sublimation and deposition of the simulated graupel surface set  
177 up by the difference in saturation vapor pressures over ice and liquid water. The transition  
178 between sublimation and deposition zones is determined from Macklin and Payne [1967] and  
179 from the Clausius-Clapeyron equation taking into account that the simulated graupel sublimates  
180 if its surface temperature becomes higher than the ambient temperature and if the equilibrium  
181 vapor pressure of ice at the simulated graupel surface temperature falls below the equilibrium  
182 vapor pressure of the environment at ambient temperature. The dot-dashed line belongs to the  
183 transition between wet and dry growth of the simulated graupel. The wet growth regimes were  
184 calculated from Macklin and Payne [1967], assuming that wet growth is reached when the  
185 surface temperature is 0 °C. It is possible to observe that the measurements were mainly  
186 performed under the dry growth regime of the simulated graupel, which was corroborated from  
187 direct observations of the surface of the simulated graupel after each measurement.

188 Figure 4 shows almost entirely negative CC at temperatures lower than -15 °C and  
189 positive CC at warmer temperatures. It suggests that under the studied conditions there is a sort

190 of charge reversal temperature for the simulated graupel ( $T_R = -15\text{ }^\circ\text{C}$ ) which is roughly  
191 independent of the liquid water content. The results indicate that precipitation ice particles of  
192 cm-sizes, under impacts with ice crystals at  $11\text{ m s}^{-1}$ , charge positively at temperatures above  $-15$   
193  $^\circ\text{C}$ , and negatively at temperatures below  $-15\text{ }^\circ\text{C}$ . These results are valid for  $0.5\text{ g m}^{-3} < \text{EW} < 5\text{ g}$   
194  $\text{m}^{-3}$  and under all these conditions the simulated graupel was mainly sublimating and in the dry  
195 growth regime. These results could be no longer valid for  $\text{EW} < 0.2\text{ g m}^{-3}$  since some researchers  
196 reported that the graupel charges positively for  $\text{EW} < 0.2$  and  $T < -15\text{C}$  [Takahashi, 1978;  
197 Saunders et al., 1991; Ávila and Pereyra, 2000; Bürgeser et al., 2006]. The range  $\text{EW} < 0.2$  was  
198 unexplored in the current study.

199 Williams et al. [1991] proposed that a simulated graupel growing by riming and  
200 sublimating simultaneously, as in the case of the current experiments, charges negatively. This  
201 hypothesis is consistent with the results at  $T < -15\text{ }^\circ\text{C}$ , but inconsistent with the results at  $T > -15$   
202  $^\circ\text{C}$ . This inconsistency was already observed in most of the previous results [Takahashi, 1978;  
203 Saunders et al., 1991; Pereyra et al., 2000; Saunders et al., 2006]. On the other hand, Baker et al.  
204 [1987] proposed that the ice-particle growing faster by vapor deposition will charge positively  
205 while the other will remain negative. In the sublimation regime, the ice-particle which sublimates  
206 slower will acquire positive charge. In the case of the present work, the ice crystals were growing  
207 by vapor deposition during the experiments because they were surrounded by supercooled water  
208 droplets (Bergeron's mechanism); while the simulated graupel was losing mass by sublimation  
209 but gaining mass due to its growth by riming. At cold temperatures, sublimation prevails over  
210 accretion so, according to the Baker's hypothesis, the simulated graupel acquires negative  
211 charge. However, as ambient temperature increases, the freezing time of the accreted water  
212 droplets increases, generating extra vapor sources onto the simulated graupel surface which

213 enhances its diffusional growth rate. At some point, the simulated graupel stops sublimating and  
214 its diffusion growth rate exceeds the ice crystal growth rate causing a change in the CC sign from  
215 negative to positive. Although this hypothesis is plausible and consistent with the current results,  
216 it still needs to be checked with more experimental evidence.

217         Regarding that the CC sign of the simulated graupel may depend on the impact velocity  
218 of the ice crystals, we compare the charge diagram obtained in the current work with those  
219 obtained by Takahashi [1978], Pereyra et al. [2000] and Bürgesser et al. [2006] who worked with  
220 velocities  $> 8 \text{ m s}^{-1}$ . Takahashi [1978] rotated a simulated graupel of 3 mm in diameter at  $9 \text{ m s}^{-1}$   
221 through an environment of supercooled water droplets and ice crystals and measured the CC of  
222 the target. He found that for  $T > -10 \text{ }^\circ\text{C}$ , the CC was positive independently of LWC values. For  
223  $T < -15 \text{ }^\circ\text{C}$  and  $0.1 \text{ g m}^{-3} < \text{LWC} < 4 \text{ g m}^{-3}$ , the sign of CC was negative. For  $-10 \text{ }^\circ\text{C} < T < -15 \text{ }^\circ\text{C}$ ,  
224 the sign of the CC depended on LWC being positive for lower and higher LWC values and  
225 negative for intermediate LWC. For instance, at  $T = -12 \text{ }^\circ\text{C}$  the CC was positive at  $\text{LWC} < 0.7 \text{ g}$   
226  $\text{m}^{-3}$  and  $\text{LWC} > 3 \text{ g m}^{-3}$ , and negative for  $0.7 \text{ g m}^{-3} < \text{LWC} < 3 \text{ g m}^{-3}$ . Beyond the behavior of the  
227 charge reversal temperature in the range  $-10 \text{ }^\circ\text{C} < T_R < -15 \text{ }^\circ\text{C}$ , the results from Takahashi [1978]  
228 looks qualitatively similar to the present results with a region of positive charging of the  
229 simulated graupel at warmer temperature ( $T > -10 \text{ }^\circ\text{C}$ ) and a region of negative charging of the  
230 simulated graupel at colder temperatures ( $T < -15 \text{ }^\circ\text{C}$ ). Pereyra et al. [2000] measured the CC for  
231 a target of 4 mm in diameter. The measurements were made for temperatures between  $-5^\circ\text{C}$  and -  
232  $30^\circ\text{C}$ , at EW values between 0 and  $4 \text{ g m}^{-3}$  and for an impact velocity of  $8.5 \text{ m s}^{-1}$ . Their results  
233 show positive CC at  $T > -17 \text{ }^\circ\text{C}$  and negative CC at  $T < -17 \text{ }^\circ\text{C}$ . Bürgesser et al. [2006] measured  
234 the sign of the CC for an artificial graupel of 4 mm in diameter during collisions with ice crystals  
235 at  $11 \text{ m s}^{-1}$ . The ambient temperature was varied in the range  $-5 \text{ }^\circ\text{C} < T < -30 \text{ }^\circ\text{C}$  and EW between

236 0 and 2 g m<sup>-3</sup>. They found a charge reversal temperature  $T_R = -15$  °C, independent of EW; the  
237 same reversal temperature occurs on both a 4 mm riming rod and a 1 cm sphere (current results).

238         Considering the similarity between the charge diagrams found by Takahashi [1978],  
239 Pereyra et al. [2000] and Bürgesser et al. [2006] and the current results, it is plausible to assume  
240 that ice precipitation particles of mm-sizes and cm-sizes are charged in similar ways during  
241 collisions with ice crystals inside thunderstorms. Most investigators currently think that the sign  
242 of the charge transfer is dependent upon the nature of the colliding surfaces [e.g. Baker et al.,  
243 1987; Williams et al., 1991; Saunders et al., 2006 and others]. The charge separation during  
244 collisions depends on the local surface state of the interacting particles. The results seem to  
245 suggest there is no apparent size effect on the local surface state for graupel of mm or cm sizes.  
246 The fact that there is no apparent size effect makes modeling simpler and narrows the parameter  
247 space for future researchers.

248         The magnitude of the average charge transferred to the target per individual ice crystal  
249 collision ( $q$ ) can be estimated by using the equation [Ávila et al, 2013]:

$$q = \frac{CC}{pE_cNVA}$$

250 Here,  $V$  is the impact velocity,  $A$  is the target cross-sectional area, and  $p$  is the probability that an  
251 ice crystal collides and bounces off the target.  $N$  is the ice crystal concentration and  $E_c$  is the  
252 collision efficiency of the spherical target for the ice crystals. Assuming that  $E_c$  of the target is  
253 the same as the glass strips used as sampler, then the factor  $E_c \times N$  can be calculated from the  
254 formvar samples. Regarding the substantial dispersion of the measurements,  $E_c \times N$  was  
255 estimated as  $(3 \pm 2)$  crystals per cm<sup>3</sup>. Furthermore, in order to calculate the average charge

256 transferred to the target, for simplicity and due to the lack of more detailed information, it was  
257 assumed  $p=1$ .

258 It was observed that the magnitude of the CC was different for the different charging  
259 regimes (positive and negative), for this reason  $q$  was estimated separately in each regime. The  
260 positive CC magnitude ranged between 1 and 14 pA. With the above assumed values for  
261 parameters in the equation, the corresponding values of positive charge transferred per  
262 rebounding collision varied between 1 and 6 fC. The negative CC magnitude varied between 1  
263 and 7 pA; therefore,  $q$  can be estimated between  $-1$  and  $-3$  fC. These values are smaller than  
264 those from Takahashi [1978], where  $q$  values were reported between 15 and 30 fC in the positive  
265 region and between  $-3$  and  $-15$  fC in the negative region. It is important to note that the ice  
266 crystals can stick the target after collisions, at least at some temperatures; which suggests that  
267 actually  $p < 1$ . Smaller values for  $p$  would increase the estimate of charge per rebounding  
268 collision and might make the values much closer to the values cited for Takahashi [1978].  
269 However, due to the lack of information about this coefficient, it is not possible to make a better  
270 estimation of  $q$ .

271

#### 272 **4. Summary and Conclusion**

273 New experimental measurements of the charge transfer during collisions between a spherical  
274 target of 1 cm in diameter growing by riming and ice crystals are reported in this work. The  
275 measurements were performed for ambient temperatures between  $-5$  °C and  $-30$  °C, for an  
276 impact velocity of  $11 \text{ m s}^{-1}$  and for effective liquid water content between  $0.5$  and  $5 \text{ g m}^{-3}$ , with

277 the goal of studying the charging behavior of ice precipitation particles of cm-sizes under  
278 microphysical conditions like those found in updrafts of deep convective clouds.

279 A charge diagram of the sign of the electric charge transfer on the ice sphere as a function  
280 of the effective liquid water content and the ambient temperature was obtained. Under the  
281 studied conditions the target was mainly sublimating and under the dry growth regime. The  
282 results indicate that precipitation ice particles of cm-sizes, under impacts with ice crystals at 11  
283  $\text{m s}^{-1}$ , are charged positively for temperatures above  $-15\text{ }^{\circ}\text{C}$ , and negatively for temperatures  
284 below  $-15\text{ }^{\circ}\text{C}$ . It suggests that under the studied conditions there is a sort of charge reversal  
285 temperature for the simulated graupel ( $T_{\text{R}} = -15\text{ }^{\circ}\text{C}$ ) which is roughly independent of the effective  
286 liquid water content in the range of 0.5 and  $5\text{ g m}^{-3}$ . Under some simplifying assumptions, a  
287 rough estimate of the average charge transferred per collision is between 1 and 6 fC in the  
288 positive charging regime and between  $-1$  and  $-3$  fC in the negative charging regime.

289 Finally, we can conclude this study extends our understanding to the larger size extreme of  
290 hydrometeors and it is useful to know how trends that have been found at smaller sizes translate  
291 to the larger sizes.

292

### 293 **Acknowledgments.**

294 We thank Secretaría de Ciencia y Tecnología de la Universidad Nacional de Córdoba (UNC),  
295 Consejo Nacional de Investigaciones Científicas y Tecnológicas (CONICET), and Agencia  
296 Nacional de Promoción Científica (PICT 2015 2644) for their support. All the data used in this  
297 work are displayed in Figures 2, 3 and 4. We thank José Barcelona for technical assistance.

298

299 **Bibliography**

300 Ávila, E. E., Varela, G. G. A., & Caranti, G. M. (1996). Charging in ice-ice collisions as a  
301 function of the ambient temperature and the larger particle average temperature. *Journal of*  
302 *Geophysical Research: Atmospheres*, 101(D23), 29609-29614.

303

304 Ávila, E. A., & Pereyra, R. G. (2000). Charge transfer during Crystal-Graupel Collisions for two  
305 different cloud droplet size distributions. *Geophysical Research Letters*, 27(23), 3837-3840.

306

307 Ávila, E. E., Lighezzolo, R. A., Castellano, N. E., Pereyra, R. G., & Bürgesser, R. E. (2013).  
308 Laboratory measurements of charge separation in low liquid water content conditions and low  
309 impact velocity. *Journal of Geophysical Research: Atmospheres*, 118(12), 6680-6687.

310

311 Baker, B., Baker, M. B., Jayaratne, E. R., Latham, J., & Saunders, C. P. R. (1987). The influence  
312 of diffusional growth rates on the charge transfer accompanying rebounding collisions between  
313 ice crystals and soft hailstones. *Quarterly Journal of the Royal Meteorological*  
314 *Society*, 113(478), 1193-1215.

315

316 Bürgesser, R. E., Pereyra, R. G., & Ávila, E. E. (2006). Charge separation in updraft of  
317 convective regions of thunderstorm. *Geophysical Research Letters*, 33(3).

318

319 Emersic, C., & Saunders, C.P.R. (2010). Further laboratory investigations into the Relative  
320 Diffusional Growth Rate theory of thunderstorm electrification. *Atmospheric Research*, 98, 327–  
321 340. doi: 10.1016/j.atmosres.2010.07.011

322

323 Heymsfield, A. J., & Kajikawa, M. (1987). An improved approach to calculating terminal  
324 velocities of plate-like crystals and graupel. *Journal of the Atmospheric Sciences*, 44(7), 1088-  
325 1099.

326

327 Jayaratne, E. R., Saunders, C. P. R., & Hallett, J. (1983). Laboratory studies of the charging of  
328 soft-hail during ice crystal interactions. *Quarterly Journal of the Royal Meteorological Society*,  
329 109(461), 609-630.

330

331 Jayaratne, E. R., & Saunders, C. P. R. (2016). The interaction of ice crystals with hailstones in  
332 wet growth and its possible role in thunderstorm electrification. *Quarterly Journal of the Royal*  
333 *Meteorological Society*, 142(697), 1809-1815.

334

335 Luque, M. Y., Bürgesser, R., & Ávila, E. (2016). Thunderstorm graupel charging in the absence  
336 of supercooled water droplets. *Quarterly Journal of the Royal Meteorological Society*, 142(699),  
337 2418-2423.

338

339 Luque, M. Y., Bürgesser, R. E. & Ávila E. E. (2018). Experimental measurements of charge  
340 separation under wet growth conditions. *Quarterly Journal of the Royal Meteorological*  
341 *Society*, 144, 842-847.

342

343 Macklin, W. C., & Payne, G. S. (1967). A theoretical study of the ice accretion  
344 process. *Quarterly Journal of the Royal Meteorological Society*, 93(396), 195-213.

345

346 Pereyra, R. G., Avila, E. E., Castellano, N. E., & Saunders, C. P. (2000). A laboratory study of  
347 graupel charging. *Journal of Geophysical Research: Atmospheres*, 105(D16), 20803-20812.

348

349 Saunders, C. P. R., Keith, W. D., & Mitzeva, R. P. (1991). The effect of liquid water on  
350 thunderstorm charging. *Journal of Geophysical Research: Atmospheres*, 96(D6), 11007-11017.

351

352 Saunders, C. P. R., Avila, E. E., Peck, S. L., Castellano, N. E., & Varela, G. A. (1999). A  
353 laboratory study of the effects of rime ice accretion and heating on charge transfer during ice  
354 crystal/graupel collisions. *Atmospheric Research*, 51(2), 99-117.

355

356 Saunders, C. P. R. (1994). Thunderstorm electrification laboratory experiments and charging  
357 mechanisms. *Journal of Geophysical Research: Atmospheres*, 99(D5), 10773-10779.

358

359 Saunders, C. P. R., & Peck, S. L. (1998). Laboratory studies of the influence of the rime  
360 accretion rate on charge transfer during crystal/graupel collisions. *Journal of Geophysical*  
361 *Research: Atmospheres*, 103(D12), 13949-13956.

362

363 Saunders, C.P.R., Avila, E.E., Peck, S.L., Castellano, N.E. and Aguirre Varela, G.G. (1999), A  
364 laboratory study of the effects of rime ice accretion and heating on charge transfer during ice  
365 crystal/graupel collisions, *Atmospheric Research*. 51, 99–117.

366

367 Saunders, C. P. R., Peck, S. L., Varela, G. A., Avila, E. E., & Castellano, N. E. (2001). A  
368 laboratory study of the influence of water vapour and mixing on the charge transfer process  
369 during collisions between ice crystals and graupel. *Atmospheric Research*, 58(3), 187-203.

370

371 Saunders, C. P. R., Bax-Norman, H., Avila, E. E., & Castellano, N. E. (2004). A laboratory study  
372 of the influence of ice crystal growth conditions on subsequent charge transfer in thunderstorm  
373 electrification. *Quarterly Journal of the Royal Meteorological Society*, 130(599), 1395-1406.

374

375 Saunders, C. P. R., Bax-Norman, H., Emersic, C., Avila, E. E., & Castellano, N. E. (2006).  
376 Laboratory studies of the effect of cloud conditions on graupel/crystal charge transfer in  
377 thunderstorm electrification. *Quarterly Journal of the Royal Meteorological Society*, 132(621),  
378 2653-2673.

379

380 Schaefer, V. J. (1956). The preparation of snow crystal replicas—VI. *Weatherwise*, 9(4), 132-  
381 135.

382

383 Takahashi, T. (1978). Riming electrification as a charge generation mechanism in  
384 thunderstorms. *Journal of the Atmospheric Sciences*, 35(8), 1536-1548.

385

386 Takahashi, T., S. Sugimoto, T. Kawano, K. Suzuki. (2017). Riming electrification in Hokuriku  
387 winter clouds and comparison with laboratory observations. *Journal of the Atmospheric*  
388 *Sciences*, 74, 431-447. DOI: 10.1175/JAS-D-16-0154.1.

389

390 Williams, E. R., Zhang, R., & Rydock, J. (1991). Mixed-phase microphysics and cloud  
391 electrification. *Journal of the Atmospheric Sciences*, 48(19), 2195-2203.

392

393 Williams, E. R. (2001). The electrification of severe storms. In *Severe Convective Storms* (pp.  
394 527-561). *American Meteorological Society*, Boston, MA.

395

### 396 **Figure captions**

397 **Figure 1.** Sketch of the experimental chamber used for laboratory studies. Droplets are produced  
398 in the cloud chamber and drawn into the target receptacle by the flow from the pump. Ice crystal  
399 produced in the adjoining chamber are inserted in the airflow just above the target.

400

401 **Figure 2.** Ice crystal size distributions for different ambient temperatures. The total number of  
402 particles (N) and the mean diameter (dm) are included in each histogram.

403

404 **Figure 3.** Droplet diameter distributions for different ambient temperatures. The total number of  
405 particles (N), the mean diameter (dm), the mean volume diameter (dv) and the median diameter  
406 are included in each histogram.

407

408 **Figure 4.** Experimental points of the rimer charge sign as a function of EW and T at  $11 \text{ m s}^{-1}$ .

409 Filled circles indicate negative charging of the rimer and open circles belong to positive results.

Figure 1.

# Cold Chamber

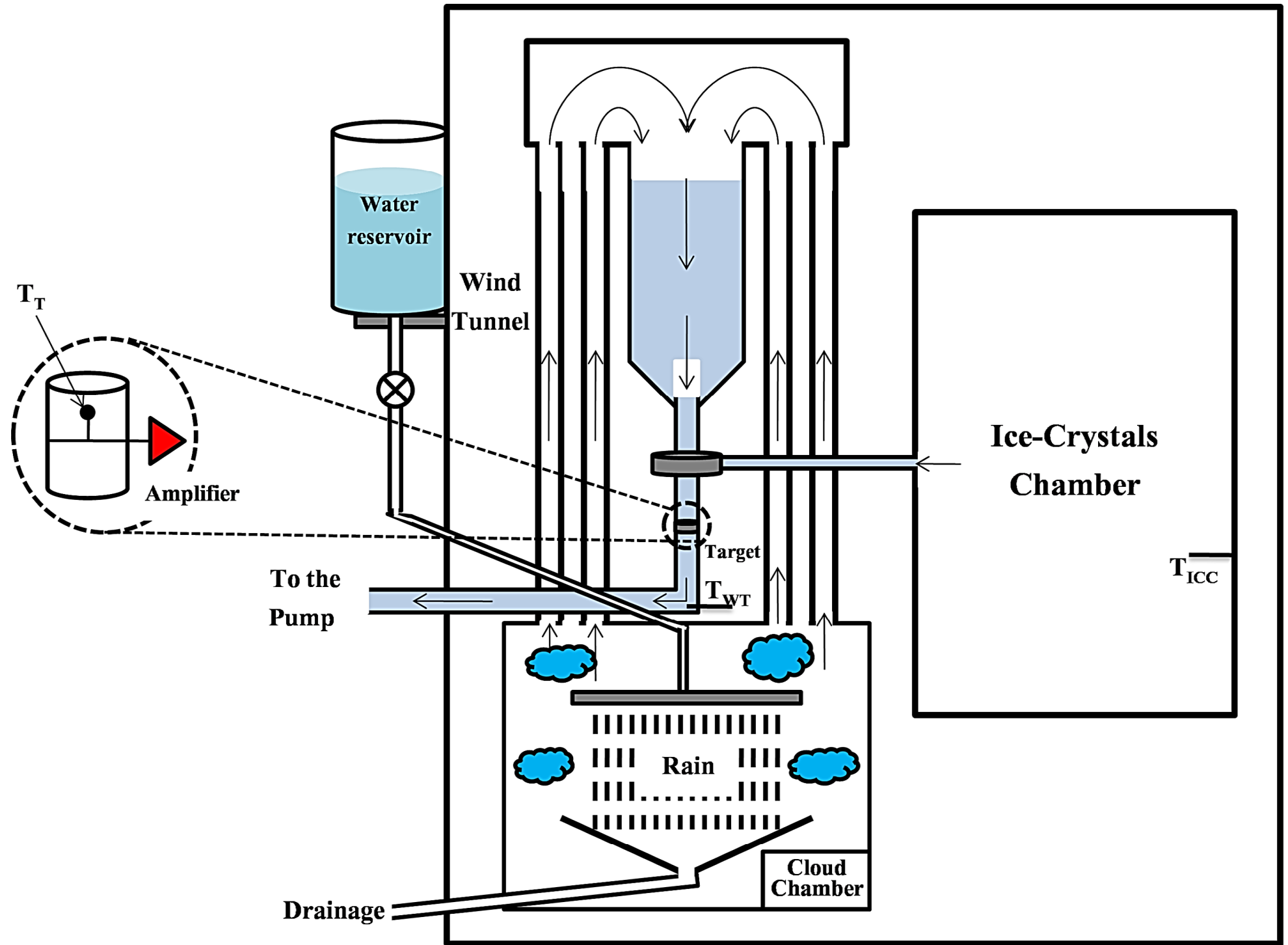


Figure 2.

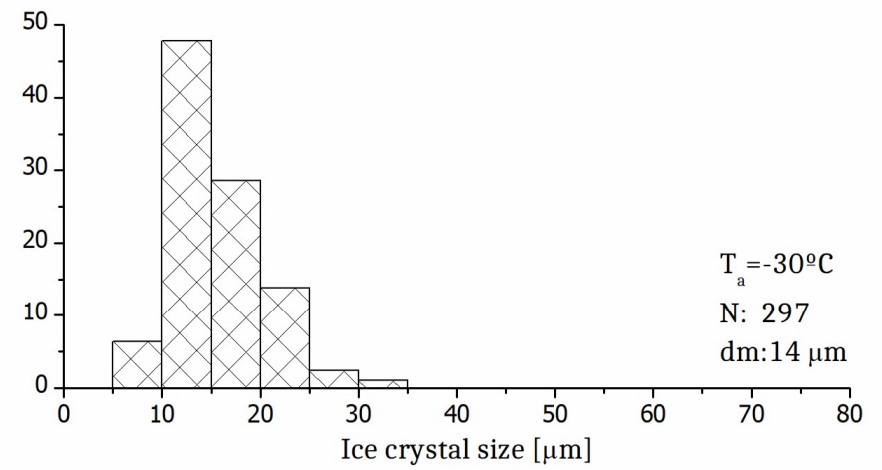
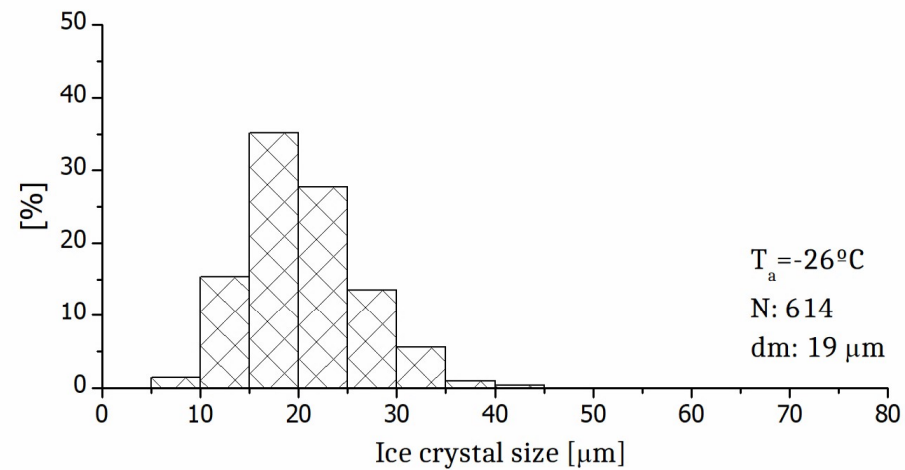
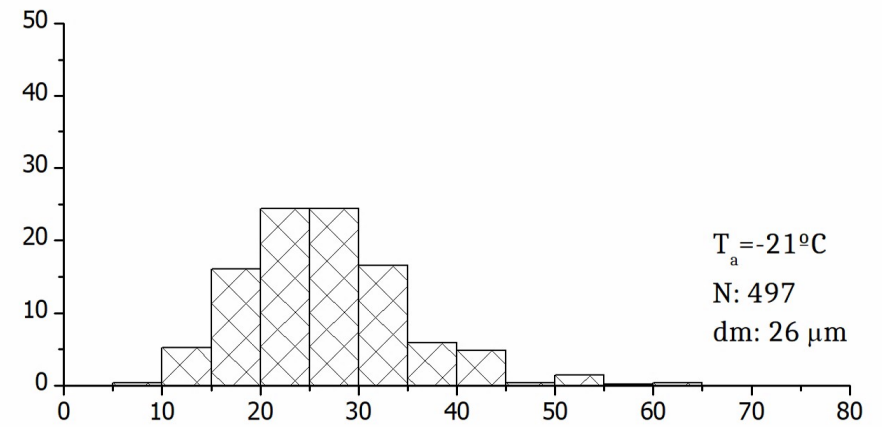
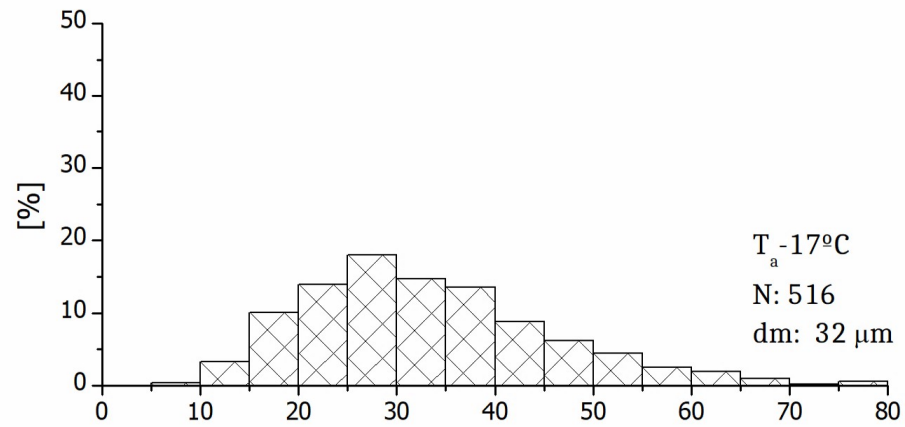
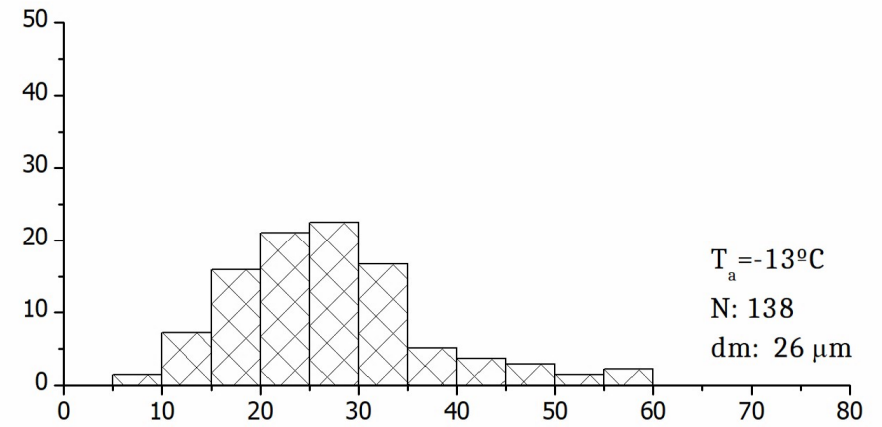
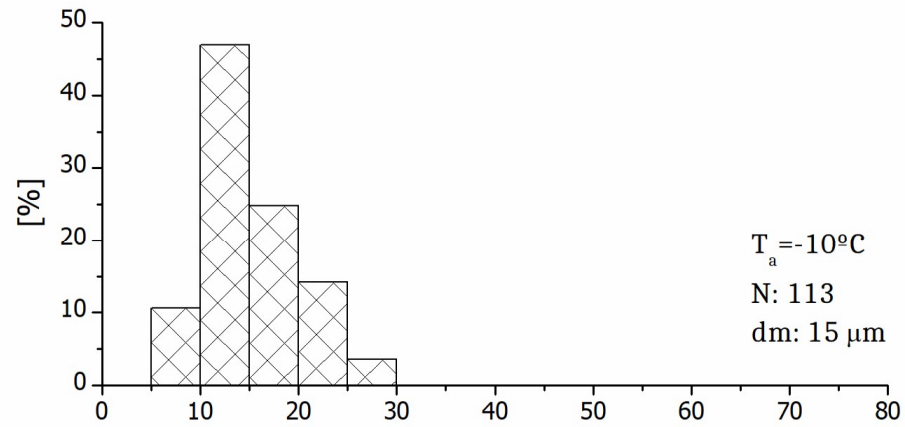


Figure 3.

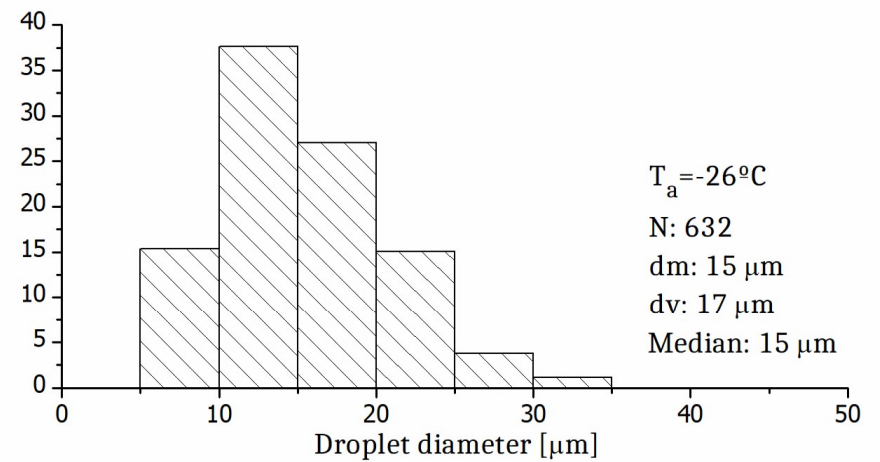
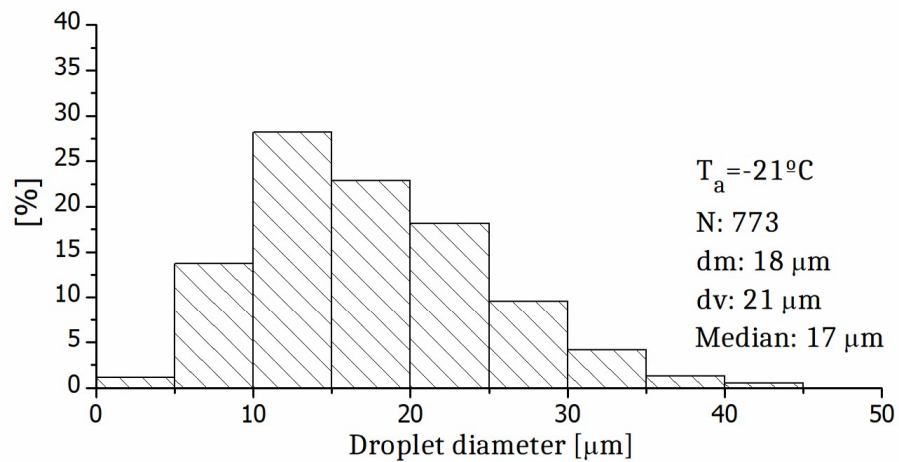
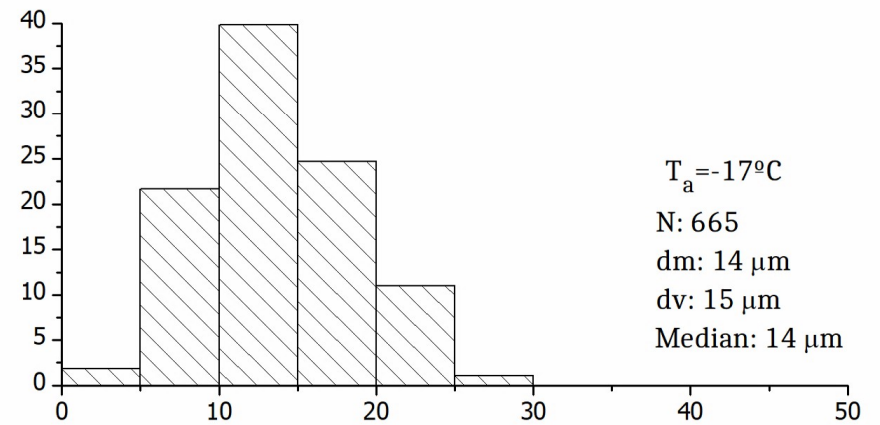
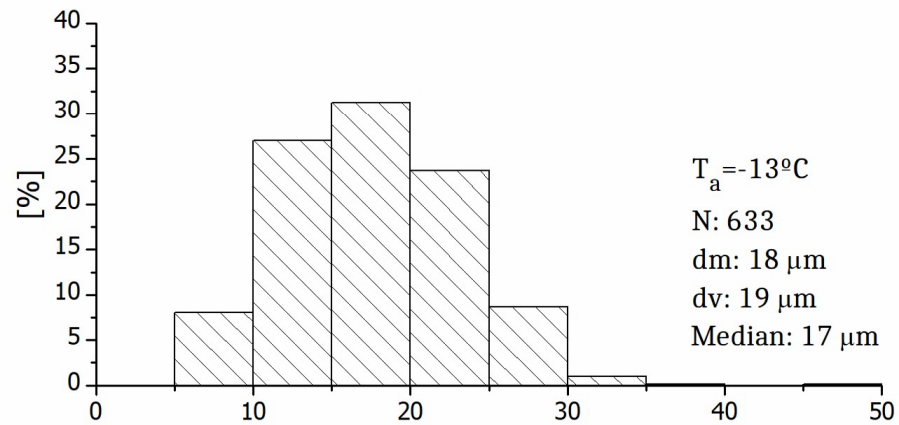
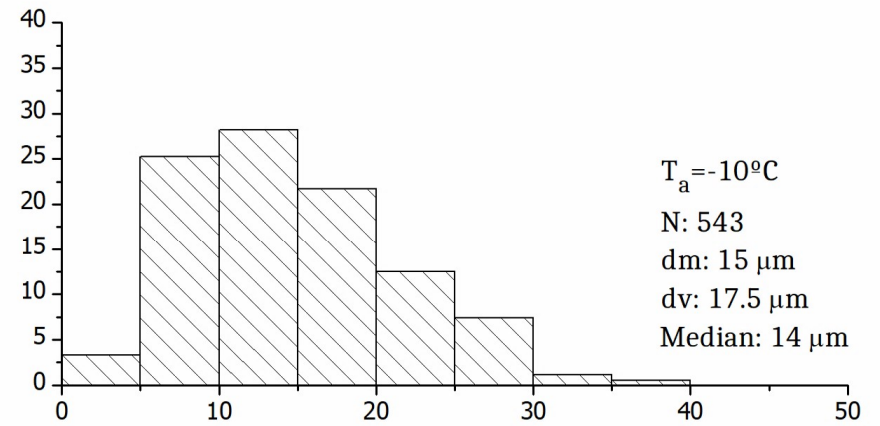
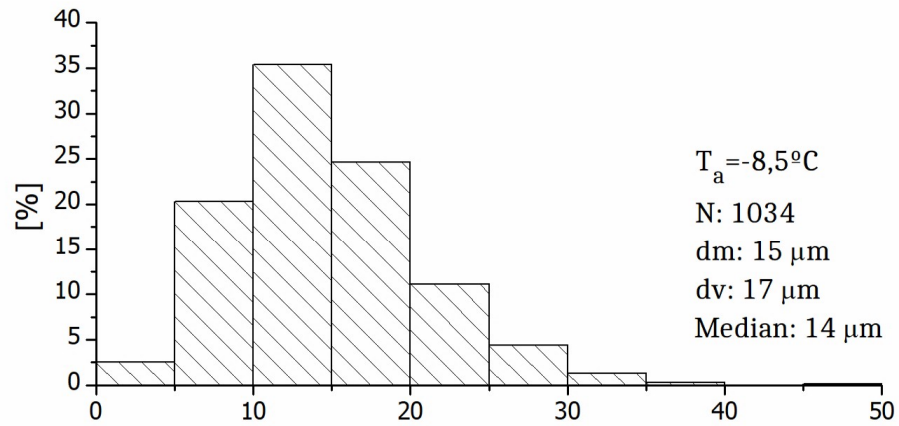


Figure 4.

